

# Statistics of Sunyaev-Zel'dovich Cluster Surveys

Andrew J. Benson, Christian Reichardt & Marc Kamionkowski

California Institute of Technology, MC 130-33, Pasadena, CA 91125, U.S.A.

19 March 2024

## ABSTRACT

We describe a detailed analytic model for predicting statistical quantities (such as number counts, redshift distributions and sizes) of clusters detected in blank-field, thermal Sunyaev-Zel'dovich effect experiments. We include in this model the possibility of non-Gaussian density perturbations in the early Universe and also describe a simple model for the effects of preheating on cluster Sunyaev-Zel'dovich effect fluxes. We use this model to explore the current state of the theoretical uncertainties present in this type of analytic modelling, highlighting where further improvement will be necessary to fully exploit forthcoming surveys. We then go on to explore the constraints on cosmological parameters, the presence of any non-Gaussianity and the degree of cluster preheating which may be obtained from both the bolocam and planck experiments. We find that, providing redshifts can be measured for all detected clusters, the bolocam experiment may provide detections of non-Gaussianity or preheating and could give approximate measurements of these effects if prior knowledge of the various cosmological parameters is taken into account. The planck experiment Sunyaev-Zel'dovich effect cluster survey is predicted to provide highly accurate ( $\sim 5\%$ ) measurements of the degree of non-Gaussianity and preheating while also providing measurements of several cosmological parameters to accuracies of a few percent independent from those constraints that will be derived from its detections of primordial cosmic microwave background anisotropies.

**Key words:** cosmology: theory, cosmic microwave background, galaxies: clusters: general

## 1 INTRODUCTION

The Sunyaev-Zeldovich (SZ) effect (Sunyaev & Zel'dovich 1972; for recent reviews see Rephaeli 1995 and Birkinshaw 1999), the distortion of the cosmic microwave background (CMB) spectrum due to the scattering of photons from electrons in hot, ionized gas (typically in clusters), is about to come of age as a cosmological probe. To date, the SZ effect has been mapped in a few clusters through targeted observations (Carlstrom et al. 2000; Joy et al. 2001), but planned experiments such as AMBA, acbar, bolocam, cbi, dasi and planck will, for the first time, carry out statistically useful surveys of clusters in the SZ effect. Since the formation rate of clusters is strongly dependent on the values of cosmological parameters we may hope to place constraints on these parameters through such SZ surveys (Thomas & Carlberg 1989; Scaramella, Cen & Ostriker 1993; Barbosa et al. 1996; Eke, Cole & Frenk 1996; da Silva et al. 2000; Refregier et al. 2000; Majumdar & Subrahmanyan 2000; Holder et al. 2000; da Silva et al. 2001; Fan & Chuah 2001; Xue & Wu 2001; Seljak, Burwell & Pen 2000; Springel, White & Hemquist 2001; Gnedin & Jahe 2001; Kay, Liddle & Thomas 2001). Furthermore, as the SZ effect probes the baryonic content

of clusters it has the potential to reveal the effects, if any, of physical processes such as feedback and preheating on the cluster gas (Majumdar & Nath 2000; Springel, White & Hemquist 2001; Majumdar, Nath & Chuah 2001).

For these reasons several studies of the SZ effect have been made recently, using both numerical methods (e.g. da Silva et al. 2000), analytic techniques (e.g. Holder, Haiman & Mohr 2001; Delabrouille, Melin & Bartlett 2001) and combinations of both (e.g. Kay, Liddle & Thomas 2001). Numerical methods have the advantage of giving a full treatment of the complex gas physics that determines the strength of the SZ signal from each cluster, but suffer from being computationally expensive. Analytic methods on the other hand are generally highly computationally efficient, but can only treat the gas dynamics in an approximate way. The ideal solution would be to build a fast and accurate analytic model tuned to reproduce the results of numerical simulations. As the first blank-field SZ surveys are expected to yield results in the next year, the time is right to explore in more detail the current theoretical uncertainties in analytic SZ models in order to highlight where further improvement is necessary. It will also be crucial to ascertain just how well proposed experiments can constrain both cosmological parameters and

the distribution of gas within clusters. In this work we will address both of these questions.

The remainder of this paper is arranged as follows. In §2 we describe our calculations of the thermal SZ fluxes of clusters. In §3 we contrast predictions for two proposed experiments, explore some of the key theoretical uncertainties in computing SZ survey statistics and derive the constraints obtainable on cosmological and gas distribution parameters in the near future. Finally, in §4 we give our conclusions.

## 2 MODEL

We begin by describing how we compute the observable properties of SZ clusters. Our model determines only the thermal SZ signal, since we do not predict the peculiar velocities of clusters needed to calculate the kinetic signal. This is not a significant problem since the magnitude of the kinetic effect is over one order of magnitude smaller than that of the thermal effect except at frequencies close to the null-point in the thermal effect spectral profile (Kay, Liddle & Thomas 2001). In §2.1 we describe the calculation of the dark-matter halo properties and in §2.2 we discuss how these halos are filled with baryonic material. Finally, in §2.3 we detail how the observable SZ properties are determined from this gas distribution.

### 2.1 Halo Distribution

We assume that dark-matter halos in the Universe can be characterised by three quantities, their mass,  $M$ , the redshift at which they formed,  $z_f$ , and the redshift at which they are observed,  $z_o$ . From these quantities we can determine, for given cosmological parameters, the virial radius and temperature of the halo from the spherical top-hat collapse model (these properties are assumed to be fixed at the formation redshift and to remain fixed until the cluster is observed). To calculate the abundance of clusters as a function of these three parameters we use the Press-Schechter theory (Press & Schechter 1974; Bond et al. 1991; Bower 1991), plus extensions described by Lacey & Cole (1993) and Sasaki (1994) that allow the distribution of formation redshifts to be determined.

The Press-Schechter theory predicts that the number of clusters of mass  $M$  to  $M + dM$  per unit comoving volume,  $V$ , observed at redshift  $z_o$  is

$$\frac{d^2 n}{dM dV} = \frac{f_{\text{crit}}}{M} \frac{\partial y}{\partial M} P(y); \quad (1)$$

where  $f_{\text{crit}}$  is the critical density of the Universe at the present day,  $y = \delta_c(z) = (\bar{M})$ , with  $\delta_c(z)$  being the critical linear overdensity for collapse at redshift  $z$  divided by the growth factor (which is normalised to unity at the present day),  $(\bar{M})$  being the linear theory mass variance at the present day in a sphere containing mass  $M$  on average,  $P(y)$  being the probability distribution function for density perturbations in the early universe and  $f = 1 = \int_0^1 P(y) dy$ . Typically,  $P(y)$  is taken to be a Gaussian (as expected from traditional models of inflation), but we will also consider other forms in this paper. This distribution is easily expressed in terms of  $z_o$  using the volume-redshift relation for Friedmann cosmologies

$$\frac{dV}{dz_o} = 4\pi r^2(z_o) c H^{-1}(z_o); \quad (2)$$

where  $c$  is the speed of light,  $r(z)$  is the coordinate distance to redshift  $z$ ,  $H(z)$  is the Hubble constant at that redshift and we have computed the volume over the whole sky. Therefore

$$\frac{d^2 n}{dM dz_o} = \frac{d^2 n}{dM dV} \frac{dV}{dz_o}; \quad (3)$$

Finally, we consider two models for the distribution of halo formation redshifts. In the model of Sasaki (1994) the fraction of clusters of mass  $M$  seen at redshift  $z_o$  which formed between redshifts  $z_f$  and  $z_f + dz_f$  is given by (Verde et al. 2001)

$$\frac{df}{dz_f} = \frac{1}{P(y_o)} \frac{dP(y_f)}{dy} \frac{\partial y}{\partial z_f}; \quad (4)$$

Therefore, the number of clusters seen in the range  $M$  to  $M + dM$ ,  $z_f$  to  $z_f + dz_o$  and  $z_o$  to  $z_f + dz_f$  is

$$\frac{d^3 n}{dM dz_o dz_f} = \frac{d^2 n}{dM dV} \frac{dV}{dz_o} \frac{df}{dz_f}; \quad (5)$$

An alternative derivation of the distribution of halo formation times due to Lacey & Cole (1993) gives the result

$$\begin{aligned} \frac{df}{dz_f} &= \frac{d}{dz_f} \int_{M/2}^M \frac{2}{M^0} \frac{y_f - y_o}{(M^0)^2 = (M)^2 - 1}^{1=2} \\ &\quad \frac{(M)^2}{(M^0)^2} \frac{d \ln}{d \ln M} \\ &\quad \exp \left[ \frac{(y_f - y_o)^2 = 2}{(M^0)^2 = (M)^2 - 1} \right] dM^0; \end{aligned} \quad (6)$$

for the case of Gaussian initial conditions. The difference between the two results is due to the different way in which "formation" is defined in the two approaches. Lacey & Cole (1993) define the formation event as that time at which a halo first had a progenitor at least half as massive as itself. Sasaki (1994) instead derives expressions for the formation and destruction rates of halos under the assumption that the destruction rate has no preferred mass scale. Figure 1 compares the two formation-redshift distributions for clusters of masses  $10^{14}$ ,  $10^{14.5}$  and  $10^{15} h^{-1} M_\odot$  (thin, heavy and very-heavy lines respectively) observed at  $z_o = 0$  in a  $\Lambda$ CDM cosmological model. Note that although the shapes of the two distributions differ, both decline rapidly at high redshifts and the mean redshift of formation becomes lower as the cluster mass (and hence  $y_o$ ) increases.

It is apparent that the two distributions are rather different, with the Lacey & Cole (1993) model predicting a much higher mean redshift of formation. The question of which is the best distribution is almost certainly problem dependent. Lacey & Cole (1994) show that their calculation accurately describes the results of  $N$ -body simulations given their definition of formation time. Note that the expression derived by Sasaki (1994) is qualitatively similar to that derived by Lacey & Cole (1993) using the mass-halving times for single trajectories, although the Lacey & Cole (1993) expression contains a dependence on the shape of the dark-matter power spectrum whereas that of Sasaki (1994) does not. However, for our work we are really interested in knowing the properties of gas in a halo. Halos of given mass that formed earlier will be denser and hotter. In reality, the pro-

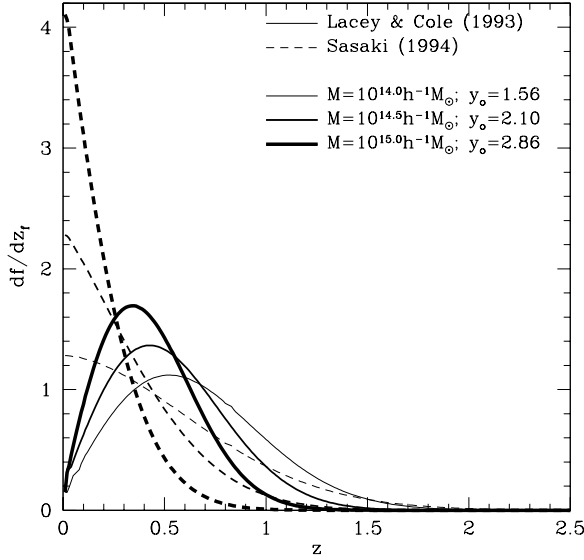


Figure 1. Comparison of formation redshift distributions. The curves show the fractional formation rate as a function of redshift for a clusters of masses  $10^{14}$ ,  $10^{14.5}$  and  $10^{15} h^{-1} M_{\odot}$  (thin, heavy and very heavy lines respectively) observed at  $z_0 = 0$  in a  $\Lambda$ CDM cosmology. The corresponding value of  $y_0$  is given for each cluster in the figure. The solid lines indicate the Lacey & Cole (1993) calculation while the dashed lines indicate the Sasaki (1994) calculation.

cess of cluster formation is a continuous one and so it is not clear just how the formation redshift should affect the gas properties. In this work we will therefore consider both distributions, and also the case of  $z_f = z_0$ . Two of these possibilities are limiting cases. The case  $z_f = z_0$  is clearly the lower limit on formation redshift, while the distribution proposed by Lacey & Cole (1993) should give a reasonable upper limit as it is difficult to see how the observed gas properties could be determined by the physical state at any earlier time (i.e. when less than half of the final mass of the cluster is in place). Our default distribution will be the Sasaki model.

With  $P(y)$  a Gaussian the Press-Schechter theory predictions differ significantly from the results of numerical simulations of structure formation (by a factor close to 2 at the characteristic mass  $M$ ). Several fitting formulae have been proposed which produce a much better agreement with numerical results. We will consider two such fitting formulae, those proposed by Sheth & Tormen (1999) and Jenkins et al. (2000) (hereafter ST and J2000 respectively), which can be described by

$$P_{ST}(y) = 0.3223 \frac{r}{2a} \left[ 1 + \frac{1}{(ay^2)^q} \exp \left( -\frac{ay^2}{2} \right) \right] \quad (7)$$

$$P_{J2000}(y) = \frac{A}{y} \exp \left( -\ln \frac{y}{1.686} + c \right)^p \quad (8)$$

where  $a = 0.707$  and  $q = 0.3$  for the ST formula and  $A = 0.301(307)$ ,  $c = 0.64(0.61)$  and  $p = 3.88(3.82)$  for the J2000 formula in the  $\Lambda$ CDM ( $\Lambda$ CDM) cosmology considered in §3.

To explore non-Gaussian initial conditions we make

use of the log-normal probability distribution proposed by Robinson, Gawiser & Silk (2000),

$$P_{RGS}(y) = \frac{f_C}{2\sqrt{A}} \exp \left( -\frac{x^2(y)}{2} \right) \delta x(y) \quad (9)$$

where  $x(y) = \ln(B + Cy\sqrt{A})/\sqrt{A}$  with  $A$ ,  $B$  and  $C$  as defined by Robinson, Gawiser & Silk (2000). The degree of non-Gaussianity is fully specified by the parameter  $A$  (with  $A = 0$  corresponding to the Gaussian limit). We will, however, characterize non-Gaussian models by the more intuitive variable  $G$ , defined by Robinson, Gawiser & Silk (2000) as the number of  $> 3$  peaks in the non-Gaussian distribution relative to the number in a Gaussian distribution (such that  $G = 1$  represents the Gaussian limit).

### 2.1.1 Cosmological Variance

The above calculations allow us to calculate the mean abundance of dark-matter halos as a function of their mass, and redshifts of observation and formation for any given cosmological parameters. However, for SZ surveys covering relatively small fields of view it is important to assess the effects of sample variance (a.k.a. cosmological variance) in order to accurately determine the ability of the survey to discriminate between models. In fact, the sample variance is expected to be rather small (close to Poissonian) since the SZ effect probes a wide range of redshifts such that any intrinsic correlations between clusters are diluted (as can be estimated using analytical calculations of the cluster bias to compute their angular correlation function). To measure the sample variance we make use of the Hubble Volume simulations which were carried out by the VIRGO Consortium and which are publicly available (Evvard et al. 1998). These large  $N$ -body simulations have been used to construct catalogues of dark-matter halos (listing their mass and observed redshift) as seen along a past lightcone.

To compute the cosmological variance from these simulations we construct mock surveys of the required angular size by choosing a random line of sight through the simulation lightcone and assigning each cluster in the field of view the SZ flux computed from our model for a cluster of the same mass and observed redshift and with a formation redshift drawn at random from the distributions described above (note that this assumes that the spatial distribution of halos of given mass and observed redshift is independent of their formation redshift, which is unlikely to be correct in detail). We then compute the statistic of interest from this mock survey. Repeating for several mock surveys we obtain a measure of the variance in the statistic. Results from these calculations will be shown in §3.3.1.

## 2.2 Baryon Distribution

### 2.2.1 No Preheating/No Cooling

Numerical simulations of gas in  $\Lambda$ CDM clusters, for example the Santa Barbara cluster comparison project (SBCCP) of Frenk et al. (1999), show that, in the absence of heating and cooling processes (other than shocks and adiabatic compression) the baryonic material of a cluster has a density profile well described by a beta model (Cavaliere & Fusco-Femiano 1976), and is close to hydrostatic equilibrium, with

a temperature at the virial radius equal to approximately half the virial temperature of the cluster. For each cluster in our calculations we determine the virial temperature from the spherical top-hat collapse model and the total mass of gas using  $M_{\text{gas}} = (b = 0)M$ . This gas is distributed in the cluster as a beta-model with  $\beta = 0.9$  and a core radius equal to 0.09 of the virial radius. We set the gas temperature at the virial radius to one half of the virial temperature and determine the temperature at smaller radii by assuming hydrostatic equilibrium. As expected, this reproduces well the profile of the SBCCP cluster. Beyond the virial radius we extrapolate the pressure and density as power-laws which also provides a good fit to the SBCCP cluster (hydrostatic equilibrium is not a good assumption here as infall is occurring).

## 2.2.2 Preheated and/or Cooled Profiles

It is well known that, in the absence of radiative cooling or any other process (other than infall-driven shocks) the relation between the X-ray luminosity and temperature of clusters differs significantly from that observed. One possible solution is that the intra-cluster medium (ICM) gas was preheated before it collapsed into the cluster, increasing its entropy and resulting in a shallower density profile. (For further discussion of these points see, for example, Tozzi 2001.)

In the case of no preheating the entropy of the cluster gas arises almost entirely from the shock it experiences as it accretes onto the cluster. If we assume that the gas is in hydrostatic equilibrium, then its "entropy" density as a function of radial distance  $r$  from the cluster centre is given by

$$K_{\text{shock}}(r) = \frac{1}{g(r)} \int_{r_{\text{vir}}}^r \frac{GM(r') g(r')}{r'^2} dr' + \frac{g(r_{\text{vir}})}{m_H} k_B T_g(r_{\text{vir}}); \quad (10)$$

where  $g$  and  $T_g$  are the gas density and temperature respectively,  $\gamma = 5/3$  is the ratio of specific heats for the gas,  $M(r)$  is the cluster mass profile,  $r_{\text{vir}}$  the cluster virial radius and  $m_H = 0.59$  the mean atomic mass appropriate to a fully ionized primordial gas (with hydrogen mass fraction  $X = 0.76$ ).

Motivated by X-ray studies (Ponman, Cannon & Navarro 1999) we introduce a minimum entropy such that the entropy profile becomes,

$$K(r) = \begin{cases} K_{\text{min}} & r < r_{\text{crit}} \\ K_{\text{shock}}(r) & r \geq r_{\text{crit}} \end{cases}; \quad (11)$$

where  $r_{\text{crit}}$  is defined by  $K_{\text{shock}}(r_{\text{crit}}) = K_{\text{min}}$ . Assuming hydrostatic equilibrium and an NFW density profile for both dark matter and shock-heated gas the corresponding density profile of the preheated gas can be obtained (by expressing the equation of hydrostatic equilibrium in terms of  $g$  and  $K$ , and then solving for  $g$ ) and is given by (S.P.Oh, private communication)

$$g(r) = \begin{cases} \frac{8}{3} \frac{h}{h_0} \frac{1}{NFW(r)} \left( \frac{1}{1 + \frac{GM_h}{r_s}} \right)^{1/2} \frac{C_{NFW}}{(1 + C_{NFW})} & r < r_{\text{crit}} \\ \frac{1}{K_{\text{min}}} \frac{\ln(1 + x_{\text{crit}})}{x_{\text{crit}}} \frac{\ln(1 + x)}{x} & r \geq r_{\text{crit}} \end{cases} \quad (12)$$

where  $C_{NFW}$  is the concentration parameter of the NFW profile (defined as the ratio of virial to scale radii and computed using the method given by Navarro, Frenk & White 1997). From this the corresponding pressure and temperature profiles are easily found. The effect of the minimum entropy is to reduce the central density and pressure of gas in halos, the effect being strongest in lower-mass halos. This necessarily reduces the SZ flux of the halos and so affects the abundances and redshift distributions of SZ selected samples. We choose to express the minimum entropy density as  $K_{\text{min}} = 10^{34} K_{34} h^{4/3} \text{ ergs cm}^{-2} \text{ g}^{-5/3}$ . Tozzi & Norman (2001) found that values of  $K_{34} = 0.12$  and  $0.25$  were required to explain the properties of groups and clusters with X-ray temperatures below and above 2 keV respectively, or alternatively that a redshift dependent value of  $K_{34} = 0.5(1+z)$  fitted the data over the whole temperature range for which data was available<sup>1</sup>.

There remains some doubt as to whether preheating is necessary at all. Dave et al. (2001) use hydrodynamical simulations which include radiative cooling to show that a good fit to the cluster X-ray luminosity-temperature relation can be achieved when cooling is included without the need for any preheating (see also Pearce et al. 2000; Bryan 2000; Muanwong et al. 2001).

Unfortunately, the effects of cooling on cluster gas profiles are more difficult to ascertain analytically, and this will be a key area in which analytic modelling must improve to fully exploit future SZ surveys to constrain the physical processes affecting cluster gas. The high-density/low-entropy inner regions of the cluster should cool in times much shorter than the Hubble time. Current evidence from numerical simulations (e.g. Pearce et al. 2000; Muanwong et al. 2001) suggests that as gas cools the surrounding higher entropy gas flows inwards to take its place. If this is indeed the case the cooling will also introduce a minimum entropy into cluster gas profiles. As such, we expect our model of preheating to produce qualitatively similar hot gas profiles to those resulting from radiative cooling. Therefore, lacking at present any better way to parameterise the effects of cooling we will consider preheated models only, and recognise that what looks like preheating may in fact be the result of radiative cooling.

## 2.3 SZ Calculation

Our calculation of the SZ flux essentially follows that of Kay, Liddle & Thomas (2001). Having determined the density and temperature profiles of the electrons in each cluster we determine the Compton parameter as a function of angular radius,  $y(\theta)$ , using

<sup>1</sup> Note that Tozzi & Norman (2001) define  $K_{\text{min}} = 10^{34} K_{34} \text{ ergs cm}^{-2} \text{ g}^{-5/3}$ , i.e. without the explicit  $h$  dependence of our definition. We have adjusted their values of  $K_{34}$  accordingly.

Table 1. Parameters of the two experiments, bolocam and planck, considered in this work.

Experiment	Solid angle (sq. deg.)	Beam FWHM	Central frequency	Frequency response	Background, $y_{bg} + 3 \sigma_{bg}$
bolocam	1	$1^0$	143 GHz	Top-hat, $\Delta\nu = 0.07$	$1.8 \times 10^{-5}$
planck	41253 (all sky)	$8^0$	143 GHz	Gaussian, $\Delta\nu = 22.5$ GHz	$1.0 \times 10^{-5}$

$$Y(\nu) = \frac{k_B T}{m_e c^2} \int_{-1}^{+1} n_e T_e dl; \quad (13)$$

where  $k_B$  is Boltzmann's constant,  $T$  is the Thomson cross section,  $m_e$  is the mass of an electron and the integral is taken along the line of sight passing a distance away from the centre of the cluster. The electron density is  $n_e = 0.88 n_H$ , where  $m_H$  is the mass of a hydrogen atom, as appropriate for a fully ionized primordial gas (with hydrogen mass fraction  $X = 0.76$ ). Although the above integral extends from  $-1$  to  $+1$ , in practice it converges with limits of order the virial radius of the halo. This profile is then convolved with a beam to mimic instrumental effects, giving

$$Y_s(\nu) = \int_{-\infty}^{\infty} Y(\nu') b(\nu - \nu') d\nu'; \quad (14)$$

where  $b(\nu)$  is the beam profile, which we take to be a Gaussian. The total SZ flux increment or decrement at frequency  $\nu$  is then found using

$$S = 2 S_0 G(x_0) \int_0^{x_b} Y_s(\nu) dx; \quad (15)$$

where  $S_0 = 2.29 \times 10^4$  mJy arcmin $^{-2}$  with  $\nu$  in arcmin and  $x_b$  is the radius at which the Compton  $y$  parameter of the observed cluster profile falls below the background. We define

$$G(x_0) = \int_0^{x_0} g(x) f(x - x_0) dx; \quad (16)$$

where  $x = h/k_B T_{CMB}$ ,  $h$  is Planck's constant,  $T_{CMB} = 2.725$  K is the mean temperature of the CMB (Mather et al. 1999),

$$g(x) = \frac{x^4 e^x}{(e^x - 1)^2} \frac{h}{x} \frac{e^x + 1}{e^x - 1} \frac{1}{4} \quad (17)$$

is the frequency dependence of the thermal SZ effect and  $f(x)$  is the filter response function, which we will take to be either a Gaussian or a top-hat.

### 2.3.1 Background

The limiting flux for SZ detections will depend upon the SZ background due to the summed contributions of all unresolved sources. This background can be characterized by a mean Compton  $y$  parameter and an rms fluctuation about this value. We can calculate the background and its fluctuations from our model using an approach similar to that described by Bartelmann (2001) (similar calculations have been used to compute the power spectrum of the SZ effect by Bruscoli et al. 2000; Valageas, Balbi & Silk 2001; Benson et al. 2001). We compute the smoothed distribution,  $Y_s(\nu)$ , for each point in the  $(M; z_0; z_f)$  plane and then determine the mean  $Y_s$ ,  $y$ , and its variance,  $\sigma^2$ , for each cluster, averaged over the whole sky. Assuming the positions of the

clusters on the sky to be uncorrelated (a good approximation as discussed in §2.1.1), the central limit theorem implies that, when the contributions from all clusters are added together, the observed mean background will be  $y_{bg} = \sum_i Y_i$  with variance  $\sigma_{bg}^2 = \sum_i \sigma_i^2$ , where the sums are taken over all clusters<sup>2</sup>.

We take the background to be  $y_{bg} + 3 \sigma_{bg}$  since below this any signal will be lost in noise due to the unresolved halos. The computed values of the background will differ between experiments, since the value of  $\sigma_{bg}$  depends upon the beam width, and also depend upon the cosmological model. (Note that our values of  $y_{bg}$  are consistent with the upper limit of  $1.5 \times 10^{-5}$  from the FIRAS instrument; Fixsen et al. 1996.) Typically we find backgrounds in the  $\Lambda$ CDM cosmology to be approximately half those in the low-density models (comparable to the results of da Silva et al. 2000). Since the effective background will depend to some degree on the particular analysis method applied to data we choose to adopt a single value of the background for each experiment (i.e. the background is assumed independent of cosmology) to permit easier comparison between models. These values are listed in Table 1.

## 3 RESULTS

We present results tuned specially to the bolocam experiment (Glenn et al. 1998) but will also consider the planck experiment (Passvogel & Felici 2000) which will survey a much larger area, albeit with lower angular resolution than bolocam. For our purposes, these two experiments differ mostly in terms of the solid angle of sky which they will survey and their beam size which determines the flux of each cluster, and also influences the background. The specific parameters used for these two experiments are listed in Table 1.

We will also consider three different cosmological models,  $\Lambda$ CDM (which is currently the most favoured observationally),  $\Omega$ CDM and OCDM. The default parameters of these models are given in Table 2 and are used for all calculations unless otherwise noted. We choose to fix the value of  $h^2$  (we define the Hubble constant to be  $H_0 = 100h$  km/s/Mpc) to 0.019 based on the results of Burles & Tytler (1998). The value of  $\Omega_8$  is fixed from the observed abundance of clusters (Eke, Cole & Frenk 1996), and the spectral shape parameter,  $\alpha$ , is chosen to match the shape of galaxy power spectra on large scales (Percival et al. 2001). All the models have a primordial power spectrum with spectral index  $n = 1$ .

We now present results for key observable properties of

<sup>2</sup> Since the distribution of  $y$  is different for each cluster the central limit theorem only applies under certain conditions (see, for example, Eadie et al. 1971), but we have checked that these apply for this particular calculation.

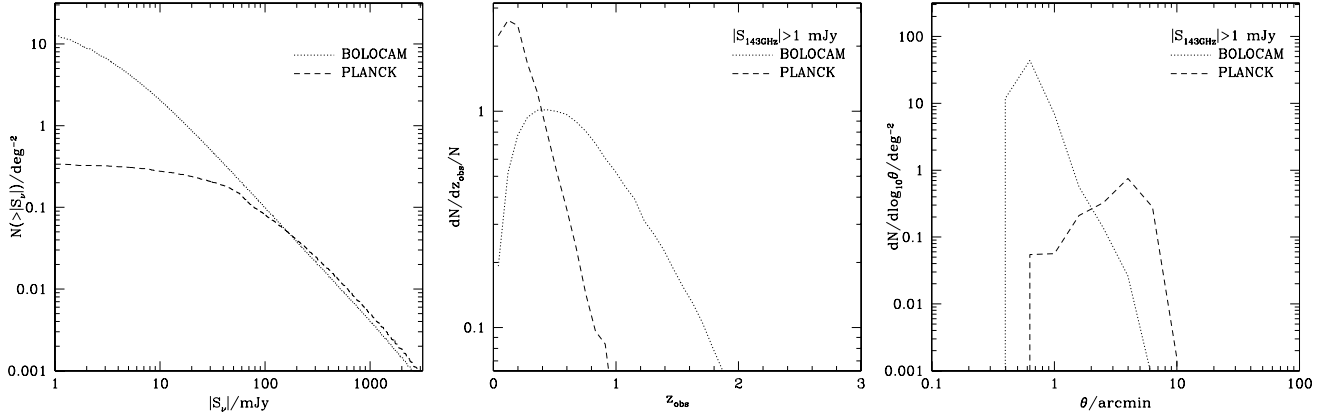


Figure 2. Properties of SZ clusters as detected by bolocam (dotted lines) and planck (dashed lines). The left-hand panel shows counts as a function of flux at 143 GHz, the centre panel shows the redshift distribution of clusters brighter than  $S_{143\text{GHz}} = 1\text{ mJy}$ , and the right hand panel shows the distribution of angular sizes for the same clusters. All results are for the  $\Lambda$ CDM cosmology with the J2000 Planck (y).

Table 2. Parameters of the cosmological models considered in this work.

Model	$\Omega_m$	$\Omega_b$	$h$	$\sigma_8$	$\Omega_k$	$w$
CDM	0.3	0.7	0.0388	0.7	0.93	0.21
CDM	1.0	0.0	0.0760	0.5	0.52	0.21
$\Lambda$ CDM	0.3	0.0	0.0388	0.7	0.87	0.21

SZ clusters. We begin by examining the differences between the bolocam and planck experiments (x3.1), proceed to explore the theoretical uncertainties in the results (x3.2.1, x3.2.2, x3.2.3), examine briefly the dependence on cosmological parameters (x3.3.1) and finally consider the effects of preheating (x3.3.3) and non-Gaussianity (x3.3.2), focusing in particular on what constraints can be put on these mechanisms and also on cosmological parameters.

### 3.1 A Case Study: BOLOCAM vs. PLANCK

We begin by briefly contrasting the two experiments that will be considered in this work. (We show results for the  $\Lambda$ CDM cosmology and the J2000 Planck (y).) Figure 2 shows three statistics of the SZ clusters that may be seen by the bolocam and planck experiments. The left panel is a plot of the number of clusters expected versus the flux limit. The middle and right panels are plots of the redshift and angular size distributions respectively for clusters with  $S_{143\text{GHz}} > 1\text{ mJy}$ . The redshift distribution is normalized by the total number of clusters brighter than this flux. (Unless noted otherwise, the format of all subsequent figures showing SZ survey statistics will be the same.)

It is immediately obvious that the smaller beam of the bolocam experiment allows it to detect many low-flux clusters which would disappear into the background for planck. As a result, bolocam should find over ten times more clusters per square degree than planck, resulting in approximately 10 SZ cluster detections per square degree. Of course, the full-sky coverage of planck will mean it detects many more clusters (several thousands) in total. Because of its greater angular resolution, bolocam will detect clusters with a

much broader redshift distribution, which will help discriminate between models with different cosmological parameters (see x3.3). Finally, the distribution of cluster sizes also reflects the size of the experimental beam in each case, with only a small fraction (approximately 10% for bolocam and 1% for planck) of detected clusters being resolved (as was noted for the planck experiment by Kay, Liddle & Thomas 2001).

Given the predicted slope of the SZ cluster counts we find that the currently proposed bolocam survey (1 square degree surveyed to a limit of 1 mJy) is close to optimal for fixed total observation time in terms of maximizing the number of detections. A slightly shallower and broader survey would detect somewhat more SZ clusters, but a deeper and narrower survey has little advantage since the cluster counts begin to turn over because the small, faint clusters begin to blend into the background due to the beam size.

Figure 3 shows which regions of the  $M_{\text{halo}}(z_f)$  plane are detectable at different observed redshifts for a  $S_{143\text{GHz}} > 1\text{ mJy}$  limited survey. Each line in the figure corresponds to a single  $z_{\text{obs}}$ , and only clusters with  $(M_{\text{halo}}; z_f)$  above and to the right of the line would be detected. It is immediately apparent that the minimum cluster mass detectable depends only weakly on the observed redshift. The dependence arises through the angular diameter distance (since the total SZ flux scales approximately as  $d_A^{-2}$  in the absence of instrumental beam effects). The minimum mass for detection is also seen to be lower for objects with higher  $z_f$  since these objects are denser and so produce larger SZ flux for given mass. (The lines become horizontal at  $z_f = z_{\text{obs}}$  since no cluster can have formed after it was observed.)

### 3.2 Assessing the Theoretical Uncertainties

In this subsection we explore the theoretical uncertainties inherent in current analytic models of SZ cluster properties. Our aim is to assess the relative importance of these uncertainties and highlight where further work is needed to produce an accurate model.

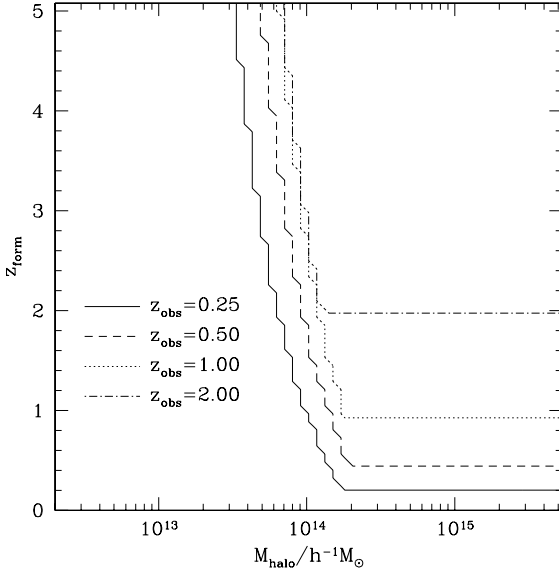


Figure 3. The regions of the  $M_{\text{halo}}(z_f)$  plane in which clusters can be detected in an  $\mathcal{J}_{143\text{GHz}} z=1\text{mJy}$  limited bolocam survey. For clusters observed at given  $z_{\text{obs}}$  (as indicated by the different line types), only those with  $(M_{\text{halo}}; z_f)$  above and to the right of the line are detected.

### 3.2.1 Sensitivity to the Mass Function

Many previous analytic studies of the SZ effect have used the Press-Schechter mass function (Press & Schechter 1974), but more accurate fitting formulae are now known. To explore the differences introduced by these alternative formulae, we have implemented both the Press-Schechter mass function and two others based upon N-body simulations developed by J2000 and ST. The J2000 mass function is currently the best match to numerical simulations over a wide range of mass scales, and should be taken as giving the best estimate of the halo mass function. We show results for the other mass functions simply for comparison.

The results for all three mass functions for the bolocam experiment are displayed in Fig. 4. The main differences between the models show up in the redshift distribution of clusters. The ST mass function produces the largest fraction of high redshift clusters while Press-Schechter produces the least (a factor of 4 fewer than ST for  $z > 1$ ). Changing the mass function also produces slight variations in the total number of clusters seen. As we will show (x3.3), an accurate redshift distribution will be crucial in determining cosmological parameters and details of the gas physics, in particular for the bolocam experiment. For that experiment, number counts alone do not contain sufficient information to be able to provide interesting constraints.

The differences between models with these three forms for  $P(y)$  as shown in Fig. 4 should be compared to the expected statistical errors from individual experiments. In the case of bolocam the statistical errors (which should be close to Poissonian – see x3.3.1) will be significantly larger than the uncertainties due to the form of  $P(y)$ . For the planck experiment however, the statistical errors will be much smaller, making the systematic differences due to the form of  $P(y)$  the dominant uncertainty.

### 3.2.2 Dependence on Formation Redshift Prescription

We next examine the effect of varying the prescription for cluster formation redshifts. The formation redshift determines the cluster's gas density and pressure, which directly impact the detectability of the cluster. This is a potentially significant effect on the number counts of SZ clusters.

At present it is not fully clear how a cluster's formation and merger histories influence the thermodynamic properties of the gas it contains. While numerical simulations may soon clarify this issue we have for now explored three possibilities for the formation redshifts of clusters (which we assume to be the thermodynamic properties of the gas as described in x2).

Comparing the predictions of the three formation redshift formulas in Fig. 5, we find that the functions proposed by Lacey & Cole (1993) and Sasaki (1994) yield quite similar results. However, the lower limit of  $z_f = z_0$  yields substantially smaller number counts. Interestingly, all three models produce remarkably similar normalised redshift distributions. It is worth noting that the differences in number counts for our three formation-redshift distributions are greater than the differences resulting from the various forms for  $P(y)$  discussed in x3.2.1, and at 1mJy become comparable to the random errors expected in the bolocam experiment. These differences highlight the need for a better understanding of how a cluster's gas properties are determined in order to make sufficiently accurate calculations of the abundance of SZ clusters, and to allow cosmological and gas-distribution parameters to be determined without systematic biases.

### 3.2.3 Dependence on Gas Temperature Profile

The form of the assumed gas density and temperature profiles will affect the calculation of the SZ flux – here we examine three temperature profiles. (Note that Kay, Liddle & Thomas (2001) explored the effect of changing the gas density profile, finding that a beta model profile as used in this work produces SZ fluxes around 40% higher than an NFW gas profile.) In our standard case, the outer boundary temperature was set by the virial theorem, the density set to a beta model, and the cluster's temperature profile calculated assuming hydrostatic equilibrium (as described in x2.2.1). Since the resulting mass-temperature relation disagrees with observations (Homer, Mushotzky & Scharf 1999), we also considered a model in which the observed mass-temperature relation was used to determine the outer boundary temperature with the temperature profile again calculated from hydrostatic equilibrium. Specifically, we used the relation given by Kay, Liddle & Thomas (2001) which was based upon the observational data of Homer, Mushotzky & Scharf (1999). Finally, the sensitivity of the SZ flux to the temperature profile was tested by using an isothermal profile. While this does not result in hydrostatic equilibrium, it should provide a useful check as to the sensitivity of the SZ flux to the temperature profile. In this case the temperature of the gas was set equal to the virial temperature of the cluster.

As seen in Fig. 6, the effects of these different temperature profiles are very small, about 20% (i.e. significantly smaller than the uncertainties due to  $P(y)$  or the formation redshift distribution, and less than the 40% differences

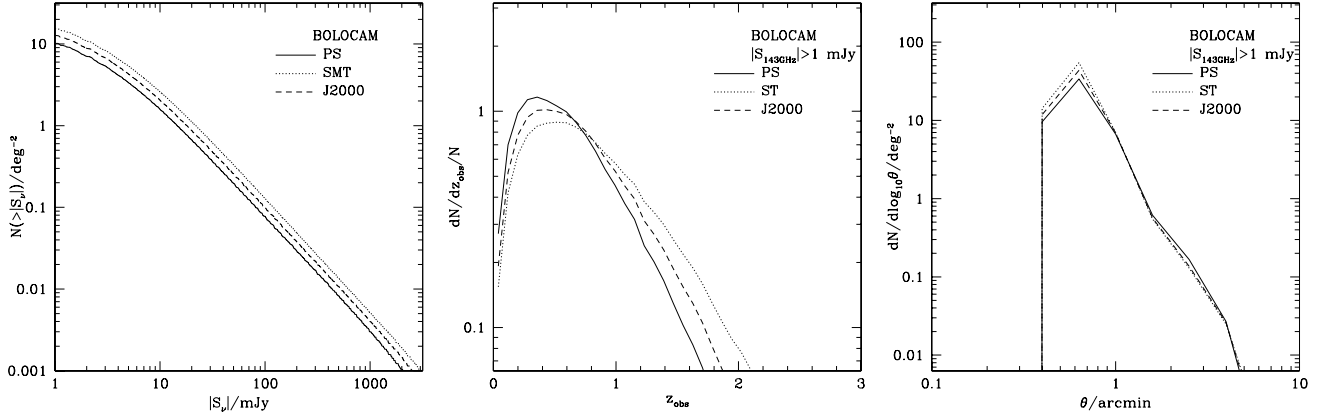


Figure 4. Properties of SZ clusters for different determinations of the halo mass function, as characterised by  $P(y)$ . Solid, dotted and dashed lines show results for the PS, ST and J2000 forms for  $P(y)$  respectively. The left-hand panel shows counts as a function of flux at 143GHz, the centre panel shows the redshift distribution of clusters brighter than  $|S_{143\text{GHz}}| = 1\text{ mJy}$ , and the right hand panel shows the distribution of angular sizes for the same clusters. (All subsequent figures will follow this general format.) All results are for the  $\Lambda$ CDM cosmology and the parameters of the bolocam experiment.

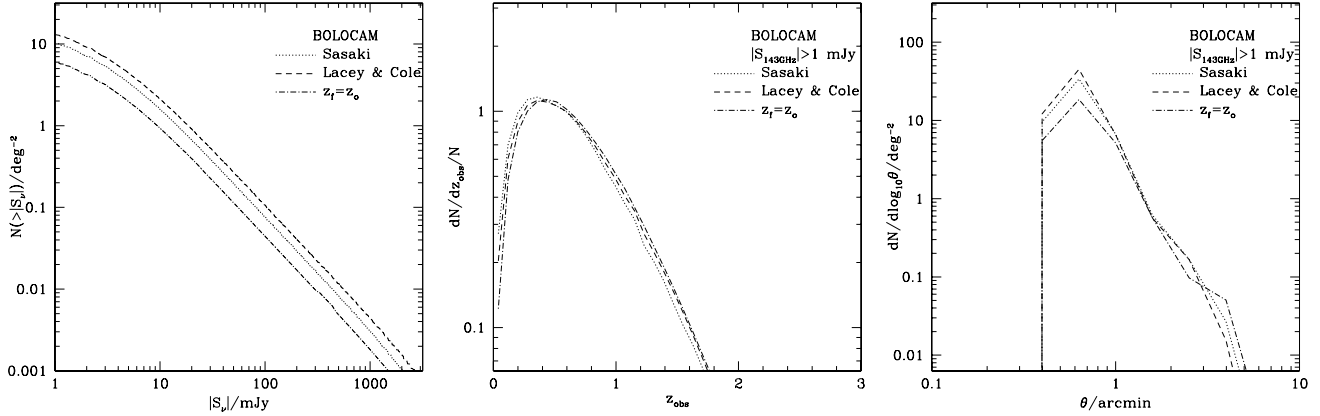


Figure 5. Properties of SZ clusters for different formation redshift calculations. Dotted and dashed lines show results for the Sasaki (1994) and Lacey & Cole (1993) formation redshift distributions respectively, while the dot-dashed line indicates the results when halos are assumed to have formed at the redshift they are observed at. The left-hand panel shows counts as a function of flux at 143GHz, the centre panel shows the redshift distribution of clusters brighter than  $|S_{143\text{GHz}}| = 1\text{ mJy}$ , and the right hand panel shows the distribution of angular sizes for the same clusters. All results are for the  $\Lambda$ CDM cosmology and the parameters of the bolocam experiment and use the J2000  $P(y)$ .

found by Kay, Liddle & Thomas (2001) for different gas density profiles), a consequence of the fact that the temperature varies only slightly with radius even in the hydrostatic equilibrium profiles. Nevertheless, improvement in this area would be necessary to fully exploit the high statistical accuracy of SZ cluster counts obtainable by the planck experiment.

### 3.3 Constraints on Cosmological Parameters, Non-Gaussianity and Preheating

#### 3.3.1 Dependence on Cosmological Parameters

It is well known that the abundance and redshift distribution of SZ clusters is sensitive to cosmological parameters as was discussed in our Introduction. Here we will briefly examine results for different cosmological parameters to demonstrate

how SZ survey statistics are affected by these quantities, and then explore the constraints that may be obtained in  $\Lambda$ CDM and  $\Lambda$ CDM.

We consider three different sets of cosmological parameters (defined in Table 2),  $\Lambda$ CDM,  $\Lambda$ CDM, and, for completeness,  $\Lambda$ CDM which is now strongly ruled out by CMB measurements (e.g. de Bernardis et al. 2001). Fig. 7 shows that there are large differences in both the total number counts of clusters and in the redshift distribution between  $\Lambda$ CDM and  $\Lambda$ CDM. As noted before, the large differences in the redshift distributions imply that obtaining redshifts for SZ detected clusters will be very valuable in helping to constrain cosmological parameters. The error bars in the left-hand panel of Fig. 7 show the rms scatter obtained from our cosmic variance calculations. As expected, the scatter is very close to Poissonian since the wide SZ redshift distribution projects out most of the clustering signal.



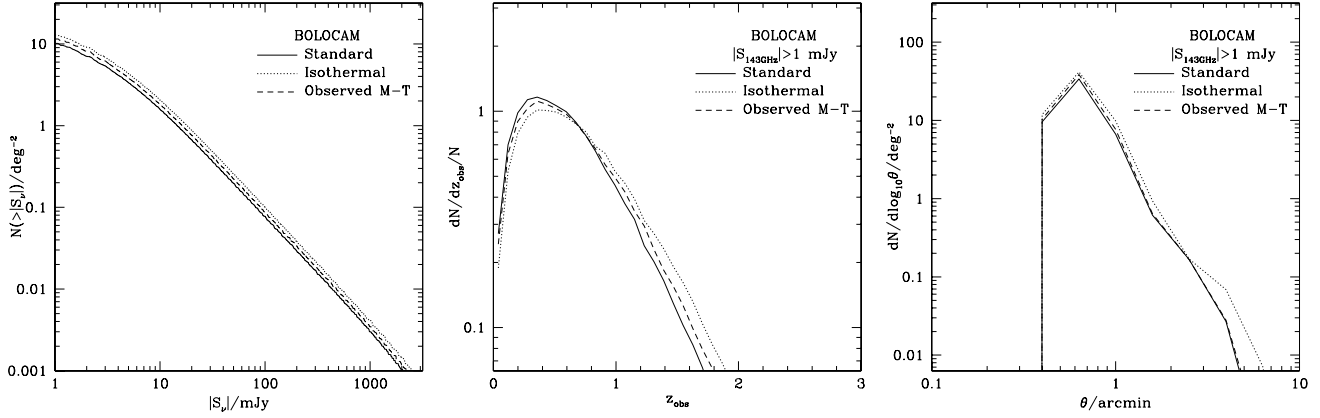


Figure 6. Properties of SZ clusters for different assumptions about the temperature profile of cluster gas. Solid, dashed and dotted lines indicate our standard assumptions, isothermal halos and halos given a temperature from the observed M-T relation respectively. The left-hand panel shows counts as a function of flux at 143GHz, the centre panel shows the redshift distribution of clusters brighter than  $S_{143\text{GHz}} = 1\text{ mJy}$ , and the right hand panel shows the distribution of angular sizes for the same clusters. All results are for the  $\Lambda$ CDM cosmology and the parameters of the bolocam experiment and use the J2000  $P(\gamma)$ .

The most significant difference is in the redshift distribution. Even a few clusters at  $z > 1$  will rule out  $\gamma_0 = 1$  in the absence of significant non-Gaussianity, providing some prior constraint on  $\gamma_8$  is adopted (since even with redshifts the constraints on  $\gamma_0$  and  $\gamma_8$  are highly degenerate, see x3.3.2). The results are also sensitive to  $\gamma_8$ . Varying  $\gamma_8$  slightly scales the number counts up and down significantly, and alters the high- $z$  tail of the redshift distribution.

The observed SZ flux will also depend on the value of  $\gamma_b$ . In our model, where the effects of radiative cooling are ignored, the electron density (and hence  $y(\gamma)$  and  $y_s(\gamma)$ ) in each dark matter halo scales in proportion to  $\gamma_b$ . Furthermore, the background which our model predicts also scales in proportion to  $\gamma_b$ . As a result of these two scalings  $\gamma_b$  in eqn. (15) is independent of  $\gamma_b$  and so the observed, integrated SZ flux of a model cluster simply scales in proportion to  $\gamma_b$ .

### 3.3.2 Constraints on Non-Gaussianity

As shown in Fig. 9, non-Gaussian initial conditions will have a large effect on both  $dN/dz$  and  $N(>S)$ . Cluster sizes are mostly unaffected. These effects are degenerate with changes due to varying several of the cosmological parameters. We will now explore quantitatively these degeneracies, and the constraints that can be placed on  $G$  and various cosmological parameters.

For the purposes of these examples, we consider only the three cosmological parameters  $\gamma_b$ ,  $\gamma_0$  and  $\gamma_8$  to be free (and assume  $\gamma_0 + \gamma_8 = 1$ ). The effects of varying  $\gamma$  may be simply scaled out of any results. These parameters are already well-measured from analysis of CMB experiments (e.g. Netterfeld et al. 2001) and cluster abundances (e.g. Eke, Cole & Frenk 1996). We will therefore adopt prior probabilities for the values of these parameters in our likelihood analysis. Each parameter is assumed to have a Gaussian prior probability distribution with a width as given in Table 3, which also lists the true value of the parameter assumed in our likelihood analysis (we choose representative values,

Table 3. The priors used to obtain constraints on  $G$  and  $K_{34}$ . For each parameter we assume a prior probability which is a Gaussian with  $\sigma$  equal to the fraction given in the table.

Parameter	"True" value	Prior accuracy
$\gamma_0$	0.3	15%
$\gamma_b$	0.04	20%
$\gamma_8$	0.9	8%

not necessarily the current best-fit values, for this analysis). For  $\gamma_0$  and  $\gamma_b$  we adopt priors based on the analysis of CMB anisotropies of (Netterfeld et al. 2001, specifically their "Flat, LSS & SN1a" determinations), while for  $\gamma_8$  we use the fractional errors obtained from cluster abundance analysis by Eke, Cole & Frenk (1996). We will show results both with and without these priors. We will take a model with  $G = 5$  as an example (note that Robinson, Gawiser & Silk (2000) were able to find a model with  $G = 10$  and low  $\gamma_8$  which produced the correct  $z = 0$  cluster abundance and also that Verde et al. (2001) demonstrated that stronger constraints could be placed on  $G$  using the observed cluster X-ray size-temperature relation).

Because of the prohibitively large amount of time required for a full analysis of the likelihood contours for model parameters obtainable from SZ surveys (even with only four parameters allowed to vary), we will illustrate likelihood contours using a Fisher matrix analysis (e.g. Jungman et al. 1996). This works well for the planck survey, where the Gaussian assumption made in the Fisher matrix analysis is justified. For the bolocam survey however, this assumption is rather poor. To demonstrate this we show in Fig. 10 the likelihood contours obtainable for a 1 square degree bolocam survey of  $S_{143\text{GHz}} > 1\text{ mJy}$  clusters, if redshifts are measured for all clusters. The thin lines indicate the results from the Fisher matrix analysis (dashed lines assume no priors, solid lines assume the priors from Table 3), marginalized over  $\gamma_0$  and  $\gamma_8$ . To compare to this, we generated a large, four-dimensional grid of models and then generated a large number of Monte-Carlo realizations of the observa-

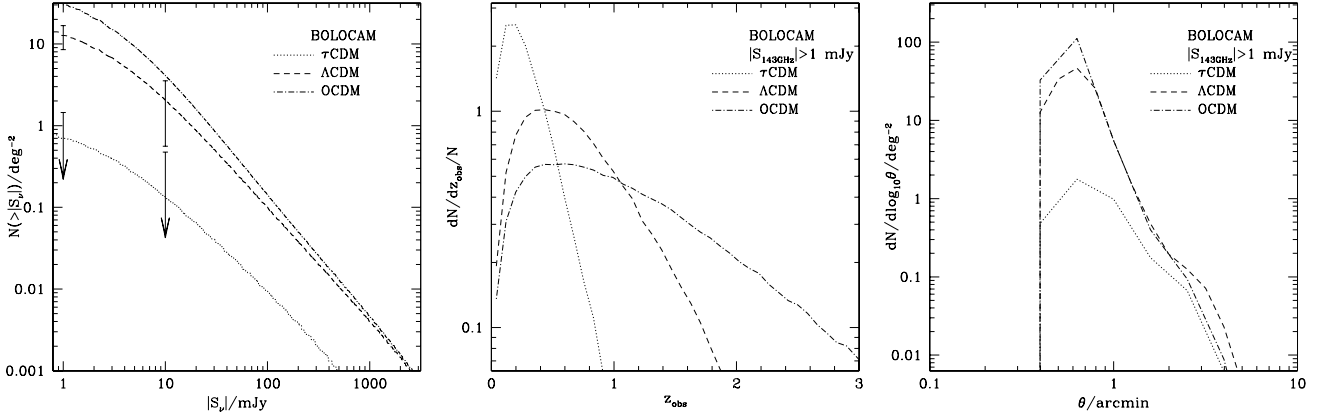


Figure 7. Properties of SZ clusters for different sets of cosmological parameters. Dotted and dashed lines show results for  $\Lambda$ CDM and  $\Omega$ CDM respectively. The left-hand panel shows counts as a function of flux at 143GHz (error bars indicate the expected cosmic variance in 1 square degree fields for the  $\Lambda$ CDM and  $\Omega$ CDM cosmologies), the centre panel shows the redshift distribution of clusters brighter than  $|S_{143\text{GHz}}| = 1\text{ mJy}$ , and the right hand panel shows the distribution of angular sizes for the same clusters. All results are for the parameters of the bolocam experiment and the J2000  $P(y)$ .

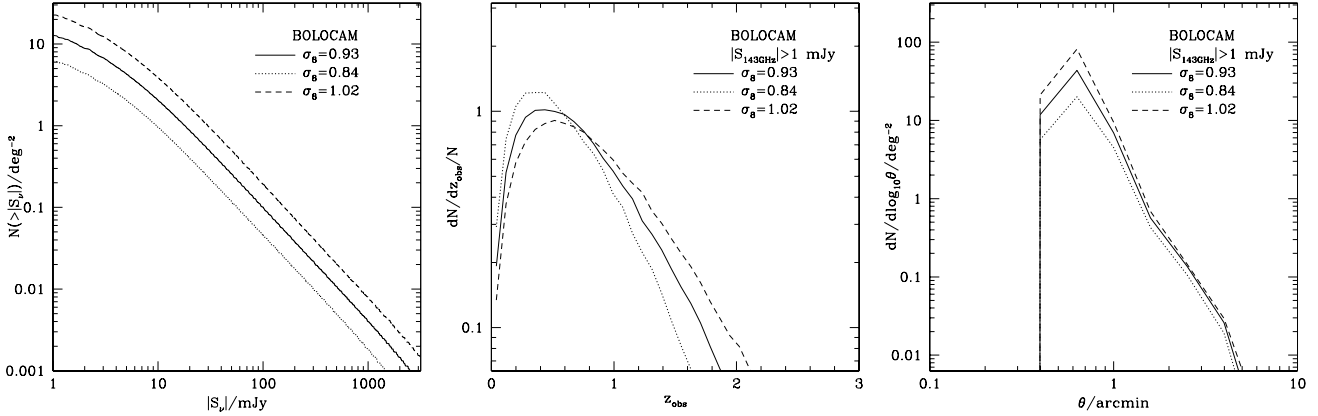


Figure 8. Properties of SZ clusters for different values of  $\sigma_8$  as indicated in the figure. The left-hand panel shows counts as a function of flux at 143GHz, the centre panel shows the redshift distribution of clusters brighter than  $|S_{143\text{GHz}}| = 1\text{ mJy}$ , and the right hand panel shows the distribution of angular sizes for the same clusters. All results are for the parameters of the bolocam experiment and the J2000  $P(y)$ .

tional dataset. The best fitting model to the mock dataset was determined using a maximum likelihood approach, and the results used to construct likelihood contours in the  $G\{y\}$  plane. It is clear that the Gaussian assumption used in the Fisher-matrix analysis is a poor approximation, with the true likelihood contours depending on the parameters in a more complex way. Nevertheless, the Fisher-matrix approach gives at least a rough idea of the constraints that can be placed on model parameters (and is very rapid to compute).

Figure 11 shows the constraints obtainable on the non-Gaussianity parameter  $G$  by the bolocam and planck experiments. In each panel we marginalize over two of the free parameters and show the error contours in the plane of the remaining two parameters. Thick and thin lines show results with and without priors (priors are included only for the bolocam experiment – for the planck experiment the priors of Table 3 do not significantly alter the confidence regions). Dashed lines indicate results when no redshift infor-

mation is available, while solid lines show results if redshifts are measured for all clusters.

It is immediately apparent that, for the bolocam experiment, no interesting constraints on  $G$  can be obtained unless either priors are assumed for the other parameters, or if redshifts are measured for all clusters (preferably both). (Note that in the left-hand panels the confidence ellipses for the case of no redshift information and no priors is so large that they lie entirely outside the regions plotted.) With full redshift information and with the priors of Table 3 we find that bolocam will measure  $G$  to an accuracy of  $\sim 40\%$  (1). (It must be kept in mind, however, that the Fisher-matrix analysis is only approximate for this survey – see Fig. 10.) Interesting constraints on the three cosmological parameters considered can also be obtained if redshifts are available for all clusters in the bolocam sample, although there are strong degeneracies between the parameters (e.g. between  $\sigma_8$  and  $\Omega_0$  in particular). The figure also demonstrates degeneracies between the various parameters, in particular be-

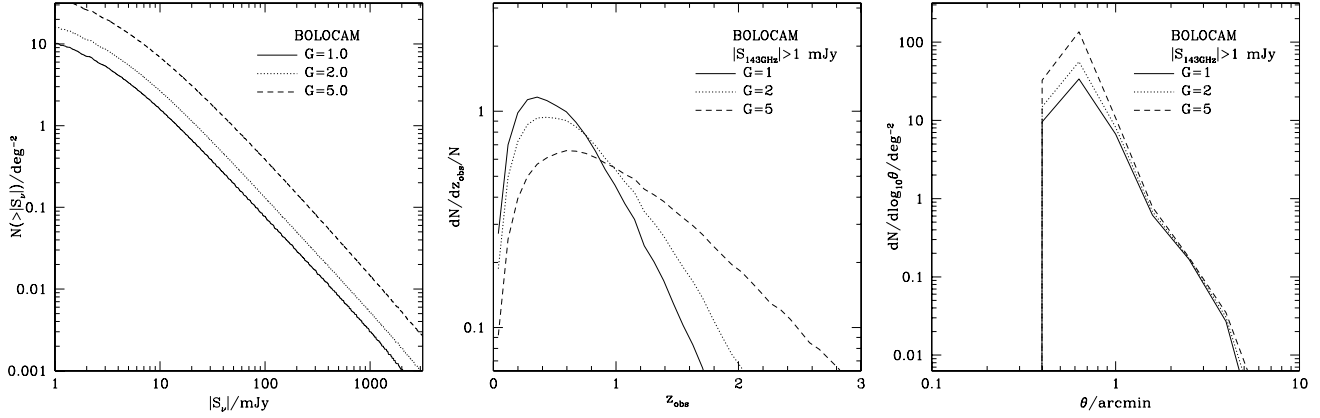


Figure 9. Properties of SZ clusters in CDM for different degrees of non-Gaussianity. Solid, dotted and dashed lines show results for the RGS P (y) using  $G = 1$  (i.e. Gaussian), 2 and 5 respectively. The left-hand panel shows counts as a function of flux at 143GHz, the centre panel shows the redshift distribution of clusters brighter than  $|S_{143\text{GHz}}| = 1\text{ mJy}$ , and the right hand panel shows the distribution of angular sizes for the same clusters. All results are for the parameters of the bolocam experiment and the CDM cosmology.

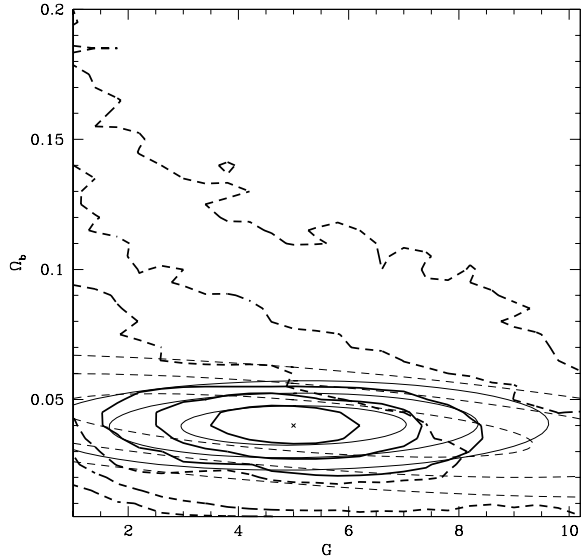


Figure 10. Constraints in the  $G - \sigma_8$  plane obtainable from the bolocam survey assuming redshifts can be obtained for all clusters brighter than  $|S_{143\text{GHz}}| = 1\text{ mJy}$ . Thin lines are the estimates from a Fisher matrix analysis, while thick lines were obtained from a large number of Monte-Carlo realizations of the dataset. Dashed lines show the results with no priors, while solid lines show results using the priors of Table 3. Contours show the 68.3%, 95.4% and 99.7% confidence regions. The cross shows the true values of the parameters.

tween  $\sigma_8$  and  $G$ . Increasing  $\sigma_8$  or  $G$  tends to increase the total number of clusters of all fluxes and also to strongly increase the numbers seen at high redshifts (see Figs. 8 and 9) leading to the degeneracy seen in Fig. 11.

For the planck experiment simple number counts of SZ clusters will constrain  $G$  to an accuracy of 5% while full redshift information would reduce that uncertainty to approximately 2% (since it is unlikely that redshifts would be available for all clusters the actual constraint on  $G$  will

lie somewhere in between these two values). Even without redshift information, the planck experiment will provide extremely tight constraints on cosmological parameters through the SZ effect (which will supplement the determinations from the primordial CMB anisotropies which are the main goal of this experiment). It should be noted that, in the case of planck the tight constraints shown here do not account for the systematic uncertainties due to theoretical uncertainties (see x3.2), which would at present be the dominant source of error.

### 3.3.3 Constraints on Preheating

Preheating of clusters will affect the total number counts (see Fig. 12 where we show results for a range of values for the minimum entropy parameter  $K_{34}$  defined in x2.2.2), by dramatically reducing the number of faint clusters, while having very little effect on the redshift distribution of SZ sources. Preheating also increases the sizes of observed clusters, producing a tail to large in the distribution of angular sizes. The effect is small and would require good statistics (and so a significantly larger survey than the 1 square degree proposed for bolocam), it is a clear signal of entropy injection since no other factor we examined has a similar effect on sizes.

Figure 13 shows confidence regions for the entropy parameter  $K_{34}$  (the form at follows Fig. 11). A gain we see that useful constraints on  $K_{34}$  from the bolocam experiment can be obtained only if redshift information is available or if priors are assumed for the various cosmological parameters. Assuming this to be the case, we find that bolocam can constrain  $K_{34}$  to an accuracy of 60%. The vastly larger area surveyed by planck will allow it to constrain  $K_{34}$  to an accuracy of 6% assuming full redshift information. Note again that the effects on SZ statistics of altering  $K_{34}$  are degenerate with changes in all three of the cosmological parameters considered in our analysis.

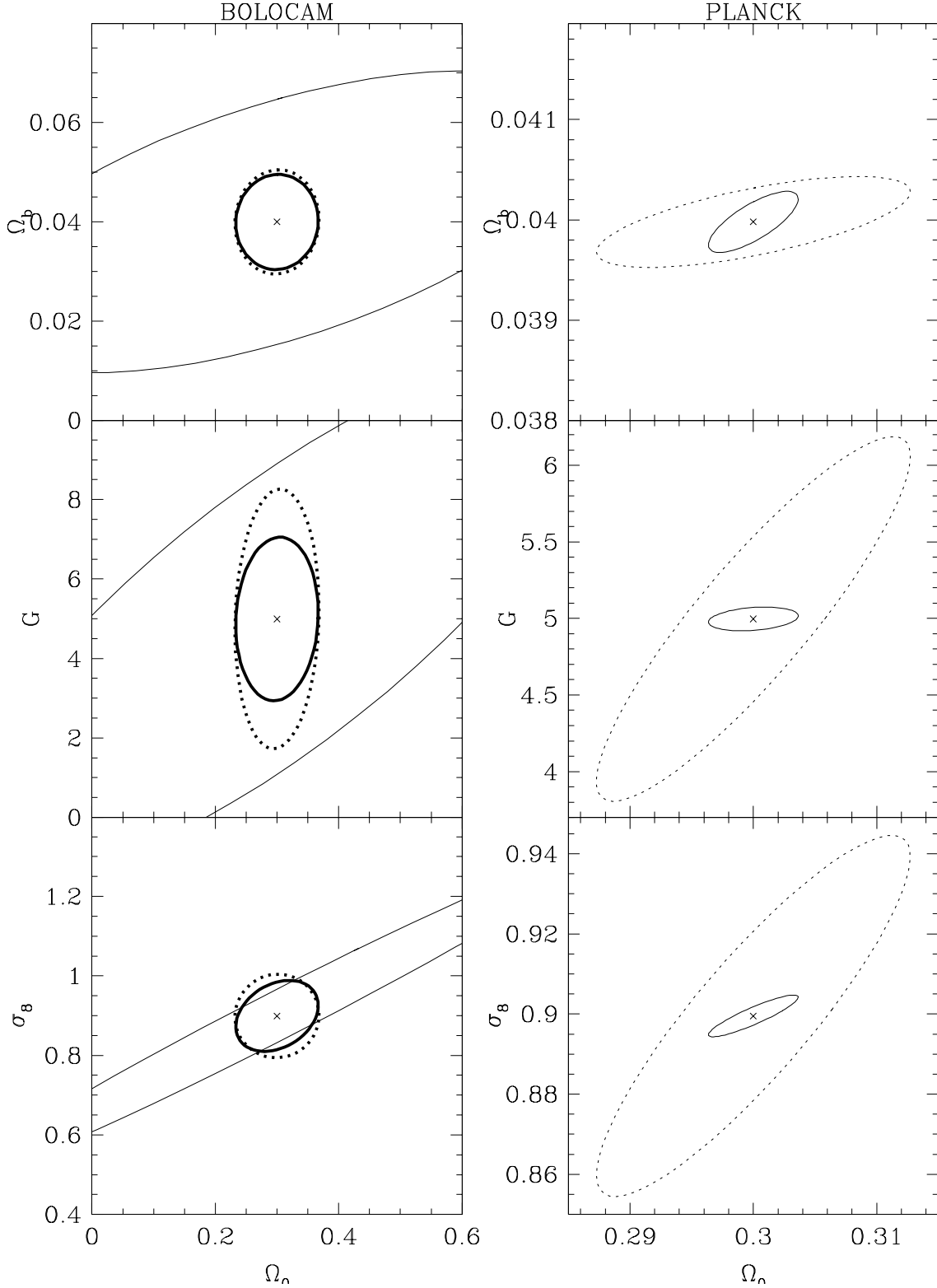


Figure 11. Left-hand panels: Joint constraints on  $\Omega_0$  and  $\Omega_b$  (top panel),  $\Omega_0$  and  $G$  (middle panel) and  $\Omega_0$  and  $\sigma_8$  (lower panel) obtainable from a 1 square degree bolocam survey to  $\mathcal{F}_{143\text{GHz}} = 1\text{mJy}$  using a Fisher matrix analysis. In each panel we have marginalized over the two parameters not shown. Thin lines show results with no priors, while thick lines use the priors from Table 3. Dashed lines make use of only the number counts of SZ clusters, while solid lines make use of their redshift distribution also (and assume that all clusters have measured redshifts). The contours show the 68.3% (i.e. 1  $\sigma$ ) confidence region. Right-hand panels: Same for a full-sky planck survey to  $\mathcal{F}_{143\text{GHz}} = 1\text{mJy}$ . Note that we do not show lines including priors for the planck experiment, since these do not significantly alter the confidence ellipses.

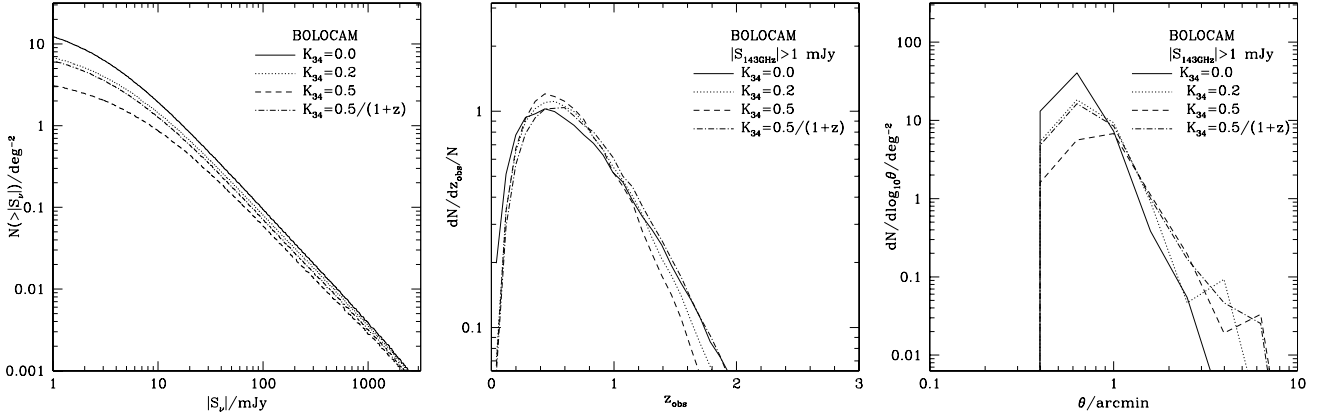


Figure 12. Properties of SZ clusters in  $\Lambda$ CDM for different levels of entropy injection. Solid, dotted and dashed lines show results for  $K_{34} = 0.0, 0.3$  and  $0.8$  respectively. The dot-dashed lines show the results when the entropy injected varies with the formation redshift according to  $K_{34} = 0.5/(1+z_f)$ . The left-hand panel shows cluster counts as a function of total SZ flux at 143 GHz, the centre panel shows the redshift distribution of clusters brighter than  $|S_{143\text{GHz}}| = 1\text{ mJy}$ , and the right hand panel shows the distribution of angular sizes for the same clusters. All results are for the parameters of the bolocam experiment and the  $\Lambda$ CDM cosmology with the J2000  $\Omega_m$  and  $\Omega_b$ .

#### 4 DISCUSSION

We have made an in-depth analysis of the statistical properties (including counts, redshift and size distributions) of clusters that should be detected through the thermal SZ effect in forthcoming experiments, in particular bolocam and planck.

Our model is based upon simple analytic calculations allowing us to explore a wide range of parameter space which is particularly important given that the details of the gas distribution within clusters are unknown, and also allows for rapid calculation of confidence regions for cosmological and gas distribution parameters. Our standard calculation consists of a distribution of dark-matter halos with a mass function matched to that found in numerical simulations and with a distribution of formation redshifts motivated by the Press-Schechter theory. These halos are filled with gas in hydrostatic equilibrium and the Compton  $y$  parameter is calculated as a function of cluster radius. Finally, we account for smearing of the cluster SZ profile by the experimental beam and then compute the observable SZ flux above the self-consistently determined background. The result is the distribution of SZ clusters as a function of total SZ flux, redshift and angular size.

We have quantified the effects of several theoretical uncertainties on the statistical quantities measurable from SZ surveys. We find that the uncertainty in how cluster formation redshifts determine the thermodynamic properties of their gas leads to an uncertainty in cluster number counts comparable to the statistical uncertainty expected for the bolocam survey. (Due to the broad redshift distributions characteristic of the SZ effect we find that sample variance is typically very small, i.e. close to the Poisson limit for the 1 square degree bolocam survey which we considered.) Other uncertainties, such as the exact form of  $\Omega_m$  and  $\Omega_b$  and the density and temperature profiles of cluster gas have slightly smaller effects, but will still dominate over the statistical errors for a full-sky planck survey. As such, it will be crucial to further our understanding of cluster gas properties before future SZ surveys can be exploited fully.

Finally, we explored the constraints that may be set on cosmological parameters and also the presence of any non-Gaussianity in the initial conditions or preheating of ICM gas in the early Universe. Redshift distributions are potentially very sensitive to  $\Omega_m$ ,  $\Omega_b$  and the presence of primordial non-Gaussianity. Preheating of clusters has much less effect on the redshift distributions but can significantly reduce the number of faint SZ clusters and also produces a tail to large sizes in the SZ cluster size distribution. A Fisher-matrix analysis reveals that bolocam will provide interesting constraints on cosmological parameters and the degree of non-Gaussianity (modulo uncertainties in  $K_{34}$ ) and/or preheating only if redshifts are measured for all the detected clusters (or if prior probability distributions are assumed for the cosmological parameters). The planck experiment, due to the large area it will survey, should measure the non-Gaussianity or preheating parameters,  $\alpha$  and  $K_{34}$  respectively, to accuracies of 5(10% even without redshifts for any of the clusters. Furthermore, the planck SZ survey will provide independent and highly accurate constraints on cosmological parameters that will complement those obtained from analysis of primordial CMB anisotropies.

In conclusion, surveys in the SZ effect will soon provide valuable measurements of various cosmological parameters which will complement measurements from other techniques. Assuming that the theoretical uncertainties highlighted in this paper can be adequately resolved, the SZ effect also has the potential to constrain the presence of non-Gaussianity and also to provide strong constraints on the distribution of gas within clusters and the presence or otherwise of any preheating.

#### ACKNOWLEDGEMENTS

AJB acknowledges helpful conversations with Scott Kay and Peng Oh. The Hubble Volume numerical simulations were kindly made available by the VIRGO Consortium. This work was supported in part by NSF AST-0096023, NASA NAG 5-8506, and DOE DE-FG 03-92-ER 40701.

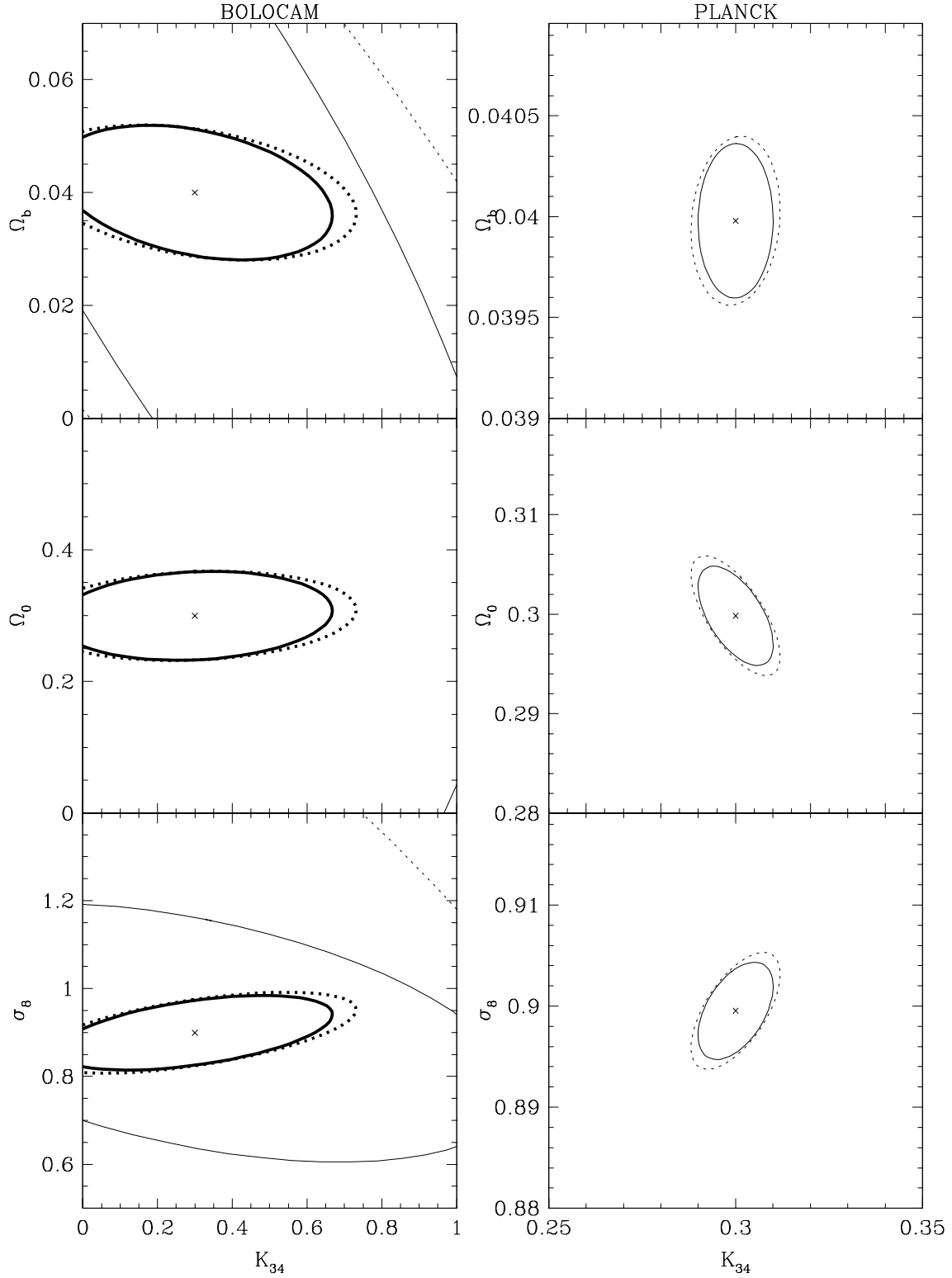


Figure 13. Left-hand panels: Joint constraints on  $K_{34}$  and  $\Omega_b$  (top panel),  $K_{34}$  and  $\Omega_0$  (middle panel) and  $K_{34}$  and  $\sigma_8$  (lower panel) obtainable from 1 square degree bolocam survey to  $S_{143\text{GHz}} = 1\text{ mJy}$  using a Fisher matrix analysis. In each panel we have marginalized over the two parameters not shown. Thin lines show results with no priors, while thick lines use the priors from Table 3. Dashed lines make use of only the number counts of SZ clusters, while solid lines make use of their redshift distribution also (and assume that all clusters have measured redshifts). Right-hand panels: Same for a full-sky planck survey to  $S_{143\text{GHz}} = 1\text{ mJy}$ . Note that we do not show lines including priors for the planck experiment, since these do not significantly alter the confidence ellipses.

## REFERENCES

- Barbosa D., Bartlett J. G., Blanchard A., Oukbir J., 1996, *A & A*, 314, 13
- Bartelmann M., 2001, *A & A*, 370, 754
- Benson A. J., Nusser A., Sugiyama N., Lacey C. G., 2001, *MNRAS*, 320, 153
- Birkinshaw M., 1999, *Phys. Rep.*, 310, 98
- Bond J. R., Cole S., Efsthathiou G., Kaiser N., 1991, *ApJ*, 379, 440
- Bower R. G., 1991, *MNRAS*, 248, 332
- Bruscoli M., Ferrara A., Fabbri R., Ciardi B., 2000, *MNRAS*, 318, 1068
- Bryan G. L., 2000, *ApJ*, 544, L1
- Burles S., Tytler D., 1998, *ApJ*, 507, 732
- Carlstrom J. A., Joy M. K., Grego L., Holder G. P., Holzapfel L., Mohr J. J., Patel S., Reese E. D., 200, *Physica Scripta*, T85, 148
- Cavaliere A., Fusco-Femiano R., 1976, *A & A*, 94, 137
- da Silva A. C., Barbosa D., Liddle A. R., Thomas P. A., 2000, *MNRAS*, 317, 37
- da Silva A. C., Barbosa D., Liddle A. R., Thomas P. A., 2001, *MNRAS*, 326, 155
- Dave R., Katz N., Hemquist L., Weinberg D., 2001, in *Proceedings of \Sesto 2001-Tracing Cosmic Evolution with Galaxy Clusters* (astro-ph/0109394)
- de Bernardis P. et al., 2001, astro-ph/0105296
- Delabrouille J., Melin J.-B., Bartlett J. G., 2001, in Chen et al. eds. *\AMiBA 2001: High-z Clusters, Missing Baryons, and CMB Polarization*, ASP Conference Series Vol. ??, p. ?? (astro-ph/0109186)
- Eadie W. T., Drijard D., James F. E., Roos M., Sandoulet B., 1971. *Statistical methods in experimenting physics*, North Holland, Amsterdam.
- Eke V. R., Cole S., Frenk C. S., 1996, *MNRAS*, 282, 263
- Evrard A., 1998, in *\Evolution of large scale structure: from recombination to Garching*, eds. A. J. Banday, R. K. Sheth, L. N. da Costa. *Garching, Germany: European Southern Observatory*, [1999] (*\Proceedings of the MPA-ESO cosmology conference, Garching, Germany, 2{7 August 1998*"), p. 249, (astro-ph/9812377)
- Fan Z., Chuieh T., 2001, *ApJ*, 550, 547
- Fixsen D. J., Cheng E. S., Gales J. M., Mather J. C., Shafer R. A., Wright E. L., 1996, *ApJ*, 473, 576
- Frenk et al., 1999, *ApJ*, 525, 554
- Glen J. et al., 1998, in Phillips T. G. ed., *Advanced Technology MMW, Radio and Terahertz Telescopes*, *Proc. SPIE*, Vol. 3357, p. 326
- Gnedin N. Y., Jaeger A. H., 2001, *ApJ*, 551, 3
- Holder G. P., Mohr J. J., Carlstrom J. E., Evrard A. E., Leitch E. M., 2001, *ApJ*, 544, 629
- Holder G., Haiman Z., Mohr J., 2001, *ApJ*, 553, 545
- Homer D. J., Mushotzky R. F., Scharf C. A., 1999, *ApJ*, 520, 78
- Jenkins A., Frenk C. S., White S. D. M., Colberg J. M., Cole S., Evrard A. E., Couchman H. M. P., Yoshida N., 2001, *MNRAS*, 321, 372
- Joy M., LaRoque S., Grego L., Carlstrom J. E., Dawson K., Ebeling H., Holzapfel W. L., Nagai D., Reese E. D., 2001, *ApJ*, 551, 1
- Jungman G., Kamionkowski M., Kosowsky A., Spergel D. N., 1996, *PhRvD*, 54, 1332
- Kay S. T., Liddle A. R., Thomas P. A., 2001, *MNRAS*, 325, 835
- Lacey C. G., Cole S., 1993, *MNRAS*, 262, 627
- Lacey C. G., Cole S., 1994, *MNRAS*, 271, 676
- Majumdar S., Subrahmanyan R., 2000, *MNRAS*, 312, 724
- Majumdar S., Nath B. B., 2000, *ApJ*, 542, 597
- Majumdar S., Nath B. B., Chiba M., 2001, *MNRAS*, 324, 537
- Mather J. C., Fixsen D. J., Shafer R. A., Mosier C., Wilkinson D. T., 1999, *ApJ*, 512, 511
- Muanwong O., Thomas P. A., Kay S. T., Pearce F. R., Couchman H. M. P., 2001, *ApJ*, 552, 27
- Navarro J. F., Frenk C. S., White S. D. M., 1997, *ApJ*, 490, 493
- Netterfeld C. B. et al., 2001, astro-ph/0104460
- Passvogel T., Felici F., in Breckinridge J. B. & Jakobsen P. eds., *UV, Optical and IR Space Telescopes and Instruments*, *Proc. SPIE*, Vol. 4013, p. 152
- Pearce F. R., Thomas P. A., Couchman H. M. P., Edge A. C., 2000, *MNRAS*, 317, 1029
- Percival et al. (The 2dFGRS Team), 2001, astro-ph/0105252
- Ponman T. J., Cannon D. B., Navarro J. F., 1999, *Nat.*, 397, 135
- Press W. H., Schechter P., 1974, *ApJ*, 187, 425
- Refregier A., Komatsu E., Spergel D., Pen U.-L., 2000, *Phys. Rev. D*, 61, 123001
- Raphaeli Y., 1995, *ARA & A*, 33, 541
- Robinson J., Gawiser E., Silk J., 2000, *ApJ*, 532, 1
- Sasaki S., 1994, *Publ. Astron. Soc. Japan*, 46, 430
- Scaramella R., Cen R., Ostriker J. P., 1993, *ApJ*, 416, 399
- Seljak U., Burwell J., Pen U.-L., 2000, *Phys. Rec. D*, 63, 063001
- Sheth R. K., Tormen G., 1999, *MNRAS*, 308, 119
- Springel V., White M., Hemquist L., 2001, *ApJ*, 549, 681
- Sunyaev R. A., Zel'dovich Ya. B., 1972, *Comm. Astrophys. Space Phys.*, 4, 173
- Thomas P., Carlberg R. G., 1989, *MNRAS*, 240, 1009
- Tozzi P., Norman C., 2001, *ApJ*, 546, 63
- Tozzi P., 2001, in *Proceedings of \Chemical Enrichment of the ICM and IGM*, Vulcano, Italy, May 2001 (astro-ph/0107150)
- Valageas P., Balbi A., Silk J., 2001, *A & A*, 367, 1
- Verde L., Kamionkowski M., Mohr J. J., Benson A. J., 2001, *MNRAS*, 321, L7
- Xue Y.-J., Wu X.-P., 2001, *ApJ*, 552, 452